ACS OMEGA

Open Access

http://pubs.acs.org/journal/acsodf

Article

Numerical Simulation Study on the Effect of Preinjected CO_2 on the Hydraulic Fracturing Behavior of Shale Oil Reservoirs

Hang Yu, Yi Ding,* Yuyang Wang, and Wenlong Zhou

Cite This: *ACS Omega* 2024, 9, 10769−10781

Read Online

ACCESS | Metrics & More | Article Recommendations

ABSTRACT: Due to the low permeability and apparent mechanical anisotropy of shale reservoirs, shale oil production highly depends on the performance of hydraulic fracturing of the tight reservoir. Pre-injection of CO_2 before hydraulic fracturing treatment has been proven beneficial to enhance shale oil production. A comprehensive understanding of the effect of changes in the properties of shale reservoirs after preinjected CO_2 on the hydraulic fracturing behavior of shale reservoirs is essential to improve the stimulated reservoir volume (SRV) of shale oil reservoirs. In this study, comprehensive evaluating parameters were proposed to specify the variation of mechanical properties of shale rock at different soaking times of CO_2 based on published testing parameters of shale. Accordingly, a three-dimensional (3D) numerical model was established and three groups of horizontal well fracturing cases with different cluster spacings were conducted based on the adaptive FE−DE method to simulate and compare the hydraulic fracturing behavior in the reservoirs with different mechanical properties. We established a quantitative relationship between the alterations in reservoir properties and the stimulated reservoir volume. The results indicate that both the brittleness and conductivity properties of shale rock are dramatically improved as the increment of soaking time of CO_2. It is beneficial to improve the SRV, and the initiation pressure is reduced with the increment of soaking time of CO_2. However, as the stress shadow effect is involved in the horizontal well fracturing, the complexity of the hydrofracturing crack is significantly enhanced to restrain the development of hydrofracturing crack. When the cluster spacing is larger, the stress shadow effect is weakened, and the weakening effect of CO_2 soaking on reservoir is more obvious.

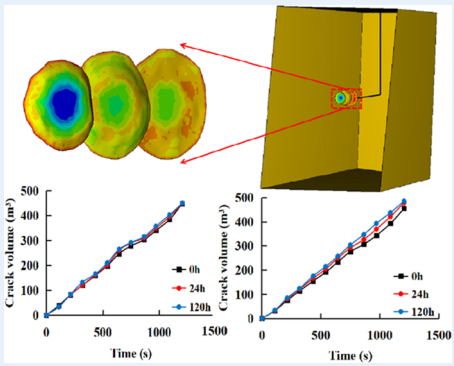

1. INTRODUCTION

Shale oil is emerging as a significant alternative energy source in response to increasing energy consumption.[1,2] The utilization of hydraulic fracturing technology has been proven effective in achieving a stable production capacity, despite the low permeability and mechanical anisotropy of shale reservoirs.[3,4] Among various techniques, hydraulic fracturing of horizontal wells stands out as the primary method for shale oil recovery.[5,6] However, it is challenging to create hydrofracturing crack networks in high horizontal stress difference, resulting in insufficient adequate stimulated reservoir volume (ESRV),[7] and cannot achieve the expected production effect of oil fields.[8] Ribeiro et al.[9] proposed an innovative CO_2-hybrid fracturing design characterized by injecting pure CO_2 to generate multiple hydrofracturing cracks in the near-wellbore zone and injecting water-based fluids to generate hydrofracturing crack conductivity to improve SRV. The oil production in Shengli and Jimusar Oilfield has also formed the CO_2 injection miscible flooding in advanced development technology of ultralow-permeability reservoir. The stimulation effect is noticeable. Based on these existing research and engineering practices, it has been demonstrated that the injection of CO_2 before hydraulic fracturing can effectively enhance oil production following the fracturing process.[10,11]

At present, the research on preinjected CO_2 in hydraulic fracturing mainly focuses on the effect of CO_2 on fluids.[12−15] Due to its advantageous characteristics, including low viscosity, high density, low surface tension, and high diffusion coefficient,[16,17] the injected CO_2 dissolves in formation water to form acidic liquid, and the acid reacts with the minerals in the reservoir to generate new minerals, thereby changing the wettability of the solid wall of the liquid phase.[18,19] Meanwhile, CO_2 enhances the extraction capacity of crude oil.[20] Its dissolution in crude oil increases the density of crude oil, reservoir volume factor, and compressibility coefficient of crude oil increase, which increases the compressibility of crude oil and further improves the productivity of oil wells.[21,22] Furthermore,

Received: December 6, 2023
Revised: February 4, 2024
Accepted: February 9, 2024
Published: February 24, 2024

within reservoir conditions, as the injection time of CO_2 increases, the injection depth into the reservoir also increases. This, in turn, leads to a rise in reservoir pressure and temperature, inducing alterations in the phase equilibrium of CO_2. These changes in the CO_2 phase state can potentially expedite the activation and propagation of pre-existing fractures.[23]However, the interaction between CO_2 and shale also has a big impact on fracturing performance. CO_2 soaking affects shale rock in various ways, such as mineral dissolution and CO_2 sorption on the rock matrix.[24,25] The degree of shale properties changed caused by CO_2 soaking is highly associated with CO_2 soaking time. Despite widespread recognition of the interaction between CO_2 and shale,[12−17] the understanding of how CO_2 soaking influences the hydraulic fracturing behavior of shale is still inadequate. However, there are rarely studies that quantitatively evaluate the impact of CO_2 soaking time on the performance of subsequent hydraulic fracturing in low-permeability shale oil reservoirs. It is important to understand the influence of these potential interactions on hydraulic fracturing performance under different soaking times.

Research at the engineering scale often involves complex physical processes and interactions, such as structural mechanics, fluid dynamics, and electromagnetic fields. These processes are often difficult to directly observe or measure through experiments, or conducting experiments may be too expensive, time-consuming, or impractical. Numerical simulation methods provide an effective approach to studying and understanding phenomena and behaviors at the engineering scale.[26] By establishing appropriate mathematical models and equations, combined with computer algorithms and numerical methods, it is possible to simulate and predict the responses and performance of various engineering systems.[27,28] Three-dimensional (3D) modeling methodologies offer superior detail in illustrating evolutionary responses when juxtaposed with two-dimensional (2D) modeling techniques. The utilization of 3D models facilitates a comprehensive examination of the interplay between fractures as well as the phenomena of nonplanar fracture deflection.[29] Sun et al.[30] proposed a numerical simulation framework for fluid flow based on a 3D fracture network induced in hydraulic fracturing laboratory experiments in their groundbreaking work. Kim et al.[31] implemented 3D simulations to model geological formations in a coupled manner, subsequently juxtaposing these simulations with empirical data derived from laboratory experiments. Their findings assert that the 3D simulation approach can accurately represent the intricacies of fluid-geomechanical systems that exhibit strong coupling characteristics. Guo et al.[32] simulated a 3D thermo-hydro-mechanical-chemical (THMC) system's response provoked by the depressurization processes in horizontal wells near the wellbore. Such simulations have substantively enriched the comprehension of the behavior within 3D-coupled THMC systems. In the present study, an adaptive finite element-discrete element (FE-DE) algorithm, encapsulated within the ELFEN software suite, was harnessed to construct a 3D simulation model. This model aims to elucidate the fracturing behaviors of shale formations after CO_2 soaking. By incorporating a model that accounts for the seepage of fracturing fluid, the effects of fluid−structure interaction, and the adaptive local remeshing strategies at crack tips, it is possible to analyze the stimulated reservoir volume of shale oil with heightened precision.[33−35]

This study aims to investigate the impact of CO_2 soaking on the behavior and performance of hydraulic fracturing. Three sets of horizontal well fracturing 3D models with different cluster spacings are conducted using the adaptive finite element-discrete element method. This approach enables the quantitative characterization of the 3D hydrofracturing crack network during fracturing, as well as the establishment of a quantitative relationship between the alterations in reservoir properties and the stimulated reservoir volume. The findings provide theoretical guidance for the implementation of on-site construction of pre-injection CO_2 fracturing.

2. NUMERICAL SIMULATION OF HYDRAULIC FRACTURING AFTER CO_2 SOAKING

2.1. The Adaptive FE-DE Simulation Method. Hydraulic fracturing is a multifield coupling process of fluid-driven rock crack. In the fracturing process of shale oil reservoirs, fracturing fluid flows through cracks, drives crack propagation, and leaks

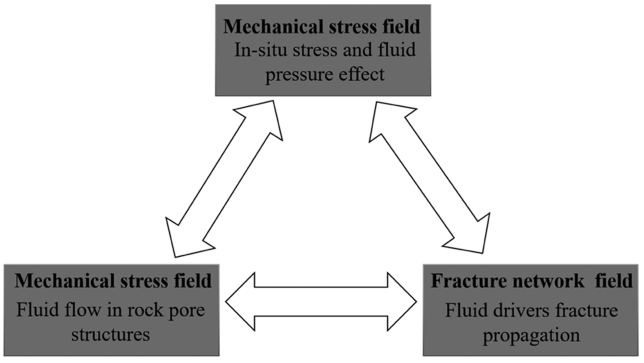

Figure 1. Fluidic-mechanical-crack coupling mechanism.

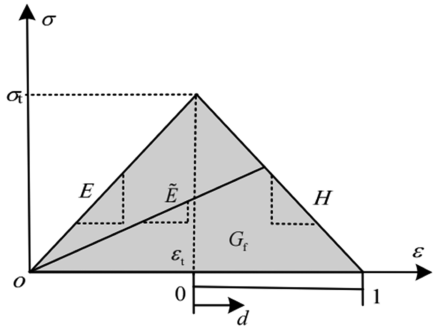

Figure 2. Relationship of stress−strain and damage analysis.

Table 1. Selection of Mechanical Parameters

	soaking time		
parameters	0 h	24 h	120 h
E (GPa)	46.45	36.98	32.72
μ	0.224	0.221	0.184
c (MPa)	8.89	8.89	8.89
Φ (deg)	47.96	47.96	47.96
σ_t (MPa)	11.47	9.48	7.71

Table 2. Selection of Permeability Parameters

	soaking time		
parameters	0 h	24 h	120 h
porosity (%)	5	7	10
permeability (10^{-18} m^2)	0.13	1.4	2.37

https://doi.org/10.1021/acsomega.3c09641
ACS Omega 2024, 9, 10769−10781

Table 3. Numerical Cases

case	reaction time of CO_2 (0 h)	reaction time of CO_2 (24 h)	reaction time of CO_2 (120 h)
I	single fracturing stage	single fracturing stage	single fracturing stage
II	25 m cluster spaces in sequential fracturing	25 m cluster spaces in sequential fracturing	25 m cluster spaces in sequential fracturing
III	50 m cluster spaces in sequential fracturing	50 m cluster spaces in sequential fracturing	50 m cluster spaces in sequential fracturing

Table 4. Basic Physical Parameters

parameter	value
horizontal minimum in situ stress in x direction Sh (MPa)	40
horizontal maximum in situ stress in y direction Sh (MPa)	46
vertical in situ stress in z direction Sv (MPa)	60
fluid injection rate Q (m^3/s)	0.5
fluid injection volume in one fracturing stage (m^3)	200
fluid injection duration in one fracturing stage (s)	400
leak-off coefficient C_I ($m^3/s^{1/2}$)	1×10^{-16}
leak-off coefficient C_{II} ($m^3/s^{1/2}$)	1×10^{-16}
pore pressure p_s (MPa)	25
initial refinement region (single-stage fracturing)	$160 \le X \le 240$
	$80 \le Y \le 120$
	$80 \le Z \le 120$
initial refinement region (multistage fracturing)	$150 \le X \le 200$
	$80 \le Y \le 120$
	$80 \le Z \le 120$

into porous media. After CO_2 is injected into the shale oil reservoir, on the one hand, the effective stress in the reservoir is changed, which leads to the alteration of permeability and porosity; on the other hand, the alteration of permeability and porosity, in turn, affect the flow and pore pressure distribution of pore fluids. Especially in the process of shale oil and gas production, continuous production of shale oil and gas, the pore pressure of the reservoir is reduced, and the solid phase stress is redistributed, which leads to the deformation of the rock skeleton of the reservoir. These changes, in turn, affect the flow of reservoir fluids in the pore space. This fluid−solid coupling effect is significant in the overexploitation of shale oil reservoirs. However, the existing numerical simulation methods are generally limited to the numerical reconstruction of the current crack network and the coupling process occurring in the known crack network, and less consideration is given to the expansion

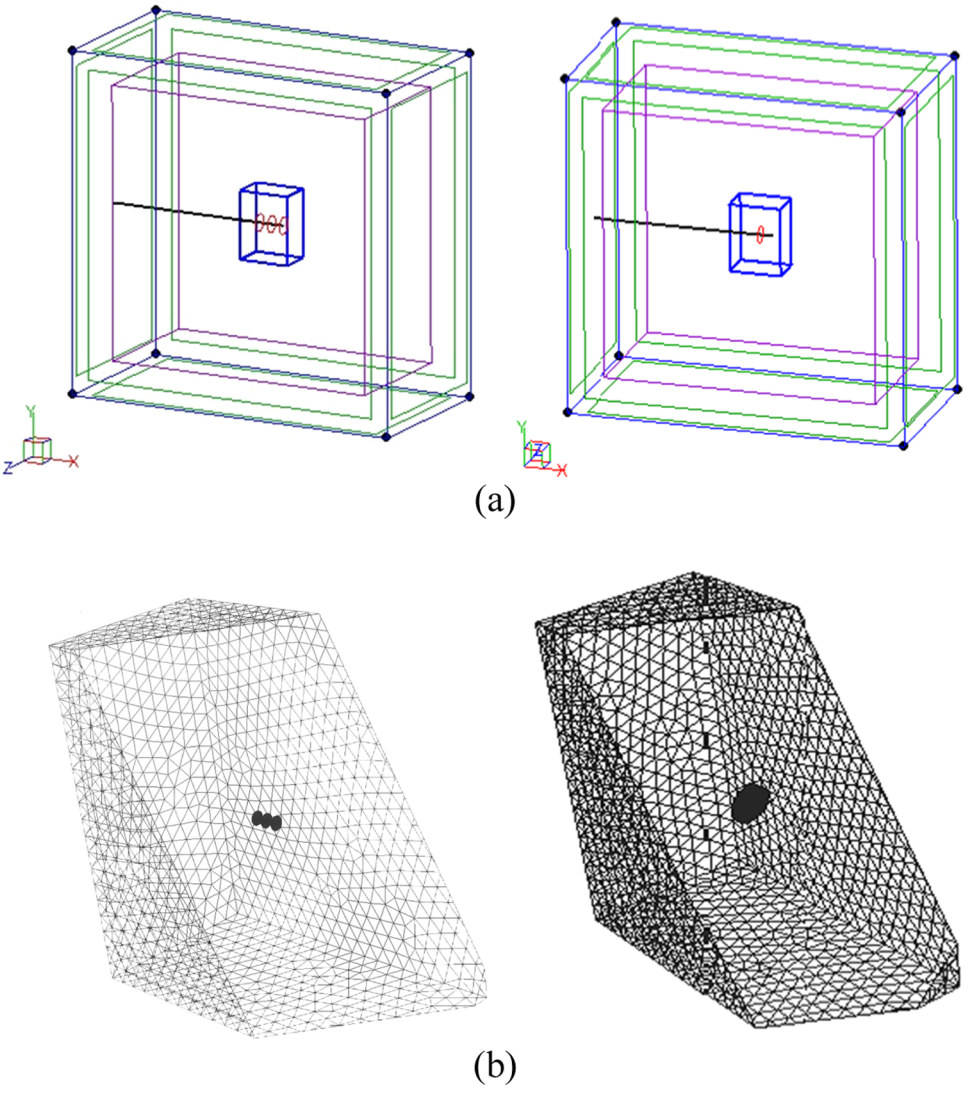

Figure 3. Numerical simulation model: (a) the geometry model and (b) the meshing model.

https://doi.org/10.1021/acsomega.3c09641
ACS Omega 2024, 9, 10769−10781

and evolution of the crack network, the instability of the network to the influence of the coupling process has also been ignored.[36] In this study, the coupling effect of fluidic-mechanical-crack was considered in the numerical simulation. The mechanical stress field acts on both the fluid pressure field and the crack network field, the fluid pressure field acts on the mechanical stress field and the crack network field, respectively, and the crack network field also acts on the fluid stress field and the mechanical stress field at the same time. The specific schematic diagram is shown in Figure 1:

2.1.1. Governing Equations for the Solid Deformation. For the solid deformation, the governing equation is[37,38]

$$L^T(\sigma^e - \alpha m p_s) + \rho_b g = 0 \tag{1}$$

where L is a time-dependent spatial differential operator, σ^e is the effective stress tensor, α is Biot's coefficient, g is the gravity vector, m is the identity tensor T, ρ_b is the saturated bulk density, and p_s is the fluid pore pressure.

2.1.2. Governing Equations for the Fluid Flow. The fluid flow equation in the rock formation and crack are[38,39]

$$\mathrm{div}\left[\frac{k}{\mu_l}(\nabla p_l - \rho_l g)\right] = \left(\frac{\varphi}{K_l} + \frac{\alpha - \varphi}{K_l}\right)\frac{\partial p_l}{\partial t} + \alpha\frac{\partial \varepsilon_V}{\partial t} \tag{2}$$

$$\frac{\partial}{\partial x}\left[\frac{k^{fr}}{\mu_n}(\nabla p_n - \rho_{fn} g)\right] = S^{fr}\frac{dp_n}{dt} + \alpha(\Delta \dot{\varepsilon}_e) \tag{3}$$

where k/kfr denotes the natural permeability, μ is the fluid velocity, ρ represents the fluid density, Kl is the pore fluid stiffness, and ε_v is the pore structure's volume strain. S^{fr} in eq 3 describes rock mass's compressibility under the fluid's action.

2.1.3. The Leak-Off Equation. When fracturing fluid is injected into the rock mass matrix, the leak-off inevitably occurs, affecting crack propagation. The following model can calculate the change of leak-off rate relative to time:[40]

$$t - t_{exp} < t_{sp} q_l = \frac{V_{sp}}{t_{sp}} \tag{4}$$

$$t - t_{exp} \geq t_{sp} q_l = \frac{C}{\sqrt{t - t_{sp}}} \tag{5}$$

where V_{sp} is the initial volume loss per unit area, t_{exp} is the time for leak-off, t_{sp} is the spurt time; q_l is the normal leak-off velocity; and C is the leak-off coefficient controlled by two parameters:[41]

$$C = \frac{2C_I C_{II}}{C_I + \sqrt{C_I^2 - 4C_{II}^2}},\ C_I = \left[\frac{k_f \phi_f \Delta p}{2\mu_f}\right]^{0.5}\Delta p,\ C_{II} = \left[\frac{k_r \phi_r \Delta p c_r}{2\mu_r}\right]^{0.5}\Delta p \tag{6}$$

2.1.4. Fracture Criteria. We introduce the damage evolution model to judge the initiation and propagation of the crack. Fracturing is initiated when the maximum principal tensile stress reaches the tensile strength. When the principal tensile stress is zero, the damage reaches the maximum. In the damage stage, the slope of the stress−strain curve and the evolution of Yong's module is given as equation. The stress−strain curve of the grid unit is shown in Figure 2. When the area enclosed by the curve and the horizontal axis reaches Gf, the rock mass is fractured.[38]

$$H = \frac{\sigma_t^2 C_l}{2G_f} \tag{7}$$

$$\tilde{E} = E(1 - d) \tag{8}$$

where σ_t is the tensile strength; C_l is the characteristic element length; G_f is the fracture energy; $\tilde{E}$ is the value of Young's modulus with damage considered; and d is the damage variable. Rock reservoirs always show strain softening with plastic damage in hydraulic fracturing shale oil reservoirs. However, in the study of this paper, the brittleness of shale oil reservoirs is enhanced after CO_2 soaking at different times. Therefore, the mechanical material model including the material damage evolution effect not only considers the problem of strain softening in the initial state of the rock reservoir but also considers the condition that the shale reservoir failure may gradually turn into elastic damage as the CO_2 soaking time increases.

2.2. Variation of Mechanical Parameters with CO_2 Soaking Time. The mechanical properties of the shale rock would be altered after CO_2 soaking. Actually, the variation of the mechanical parameters of shale rock relating to CO_2 soaking has been widely studied. According to published data, three groups of shale rock's mechanical parameters under different soaking times were collected, as shown in Table 1.[42−44] It is shown that both the elastic modulus and Poisson's ratio decline with the increment of CO_2 soaking time. However, the parameters of internal friction angle and cohesion rarely vary with CO_2 soaking.[43] Thus, the varied elastic modulus and Poisson's ratio were arranged for the numerical model in different scenarios, while the internal friction angle and cohesion remain constant.

The Biot coefficient is related to the porosity elasticity. It is required in this numerical model to establish the interaction bridge between fluid flow and solid deformation in a porous medium. Even with unconventional reservoirs, particularly shale formations, the availability of experimental data on porosity elasticity is severely limited, leading to significant variations in the published Biot coefficients depending on the specific rock type and lithology under consideration. Consequently, in our model, we adopt a novel approach proposed by Li et al. to estimate the correlation for the Biot coefficient, which relies on permeability and porosity. This correlation demonstrates applicability across a broad range of permeabilities and porosities, rendering it well suited for unconventional reservoirs like tight shale. The corresponding empirical formula is presented as eq 9.[45]

$$\alpha = 0.08258 \times \ln 2.665 \times \left[\frac{k}{(100\Phi)}\right]0.45 + 0.60685 \tag{9}$$

where k and Φ refer to the permeability and porosity of the shale under different CO_2 soaking times, respectively. Thus, the variation of permeability and porosity with the CO_2 soaking were also collected from published data as shown in Table 2. Accordingly, the corresponding Biot coefficient values are 0.57, 0.63, and 0.64, respectively.

2.3. Numerical Model. In this study, the numerical model with the geometric of 200 m × 200 m × 40 m was conducted to study the hydraulic fracturing behavior after different times of CO_2 soaking in the horizontal well fracturing scheme. Moreover, both single-stage fracturing and multistage fracturing were implemented in the numerical simulation to investigate the effects of stress shadow, as shown in Table 3. Figure 3 shows the geometry and initial mesh models for single-stage and multiple-

https://doi.org/10.1021/acsomega.3c09641
ACS Omega 2024, 9, 10769−10781

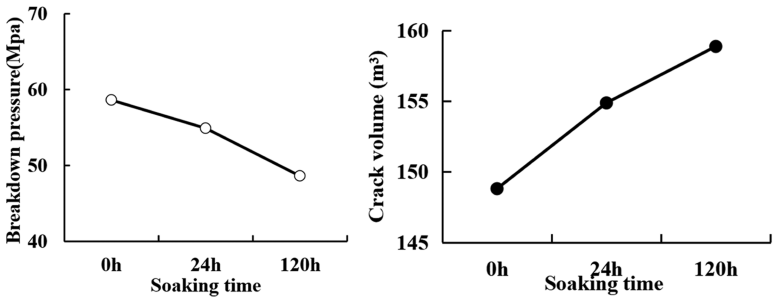

(a) Breakdown pressure (b)Final hydrofracturing crack volume

Figure 4. (a) Breakdown pressure and (b) final hydrofracturing crack volume.

stage fracturing. Other physical parameters of these three simulation scenarios are listed in Table 4.

3. RESULTS AND DISCUSSION

3.1. Single-Stage Horizontal Well Fracturing. Figure 4 illustrates the breakdown pressure and crack volume under the impact of CO_2 at different times. The breakdown pressure exhibits an almost linear decrease as the CO_2 soaking time increases. Specifically, after 24 and 120 h soaking, the breakdown pressure was reduced by 6 and 17% respectively. Moreover, the rate of breakdown pressure decreases is more rapid as the soaking time extends from 24 to 120 h. In the same injected fracturing fluid volume, Figure 4b shows that the stimulated reservoir volume linearly increases with the increment of CO_2 soaking time. The crack volume was reduced by 4 and 7%, respectively, after a soaking time of 24 and 120 h. As a result of CO_2 soaking, it is easier to initiate and propagate cracks in shale reservoir and the stimulated reservoir volume (SRV) experiences a significant enhancement.

Figure 5 illustrates the evolution of the 3D morphology of hydrofracturing crack networks after different CO_2 soaking times. It is observed that all cracks propagate along their initial perforation, resulting in an almost planar 3D morphology. In the process of hydrafracturing, it is evident that the unstable expansion phenomenon of the shale reservoir after CO_2 soaking is very obvious although the crack continues to expand in all three cases. At 105s and 205s, the crack networks in the original reservoir are significantly larger than that of the CO_2-soaked reservoir. However, at the later stage of fracturing, the crack networks in the CO_2-induced reservoir experience a sudden and much larger increase. This phenomenon of unstable expansion becomes more pronounced as the duration of CO_2 soaking increases. Additionally, the final volume of hydrofracturing cracks is significantly enhanced with a CO_2 soaking time of 120 h. Throughout different stages of hydraulic fracturing, the principal stress within CO_2-soaked reservoirs exhibits a decreasing trend, which becomes more obvious with longer soaking times. Simultaneously, it is apparent that the core of the morphology of crack experiences negative principal stress, while the periphery undergoes positive principal stress, resulting in tensile failure. In the initial reservoir, the distribution of positive principal stress surrounding the morphology of crack is nonuniform, causing the crack to propagate longitudinally. However, in the reservoir following 120 h of CO_2 soaking, the positive principal stress surrounding the hydrofracturing crack is uniformly distributed at 405s. Consequently, the hydrofracturing crack propagates evenly in all directions, leading to an increased volume of the reservoir after soaking.

3.2. Multistage Horizontal Well Fracturing. To investigate the stress shadow effects and the influence of CO_2 on hydrofracturing crack propagation, two different cluster spacings were considered in the fracturing scenarios labeled as II and III. Figure 6 shows the evolution of hydrofracturing crack volume under 25 and 50 m cluster spaces in sequential fracturing. With the increase in time, there is a continuous increase in the volume of hydrofracturing cracks. When the cluster spacing is set at 25 m, the disparity in the evolution of crack volume before and after CO_2 soaking is minimal. However, under a cluster spacing of 50 m, the initial stage demonstrates similar patterns of crack growth and evolution before and after CO_2 soaking. Nevertheless, the volume of crack volumes after soaking experiences sudden instability and rapid escalation, leading to a noteworthy surge in the final volume beyond 700 s. Figure 7 shows the final propagation volume of cracks under the sequential under 25 and 50 m cluster spaces. Under 25 m cluster spaces, there was no significant increase in crack volume with the increase of CO_2 soaking time in the same injected fracturing fluid volume. After 24 h of soaking, the crack volume increased by 2.2‰, and after 120 h, it increased by 3.5‰. However, under 50 m cluster spacing, the crack volume clearly increases with longer CO_2 soaking time. Nevertheless, the growth increment is not linear: after 24 h of soaking, the rate of increase accelerates significantly, accounting for 5.3% of the initial value. After 120 h, although the growth is obvious, it is smaller than that of 24 h, representing 6.9% of the initial value.

The findings from the evolution of crack volume demonstrate that the behavior of crack volume and the interaction between cracks becomes complex due to the stress shadow effect and CO_2 action. When the cluster spacing is small, the stress shadow effect becomes prominent, leading to strong mutual interference between hydrofracturing cracks, which hinders their propagation. However, as the cluster spacing increases, the mutual interference between g cracks diminishes significantly. While CO_2 soaking enhances the stress shadow effect, it has little influence on the mutual interference between cracks. Consequently, the volume of hydrofracturing cracks maintained an upward trend after CO_2 soaking, indicating that CO_2 preinjected improved the stimulation reservoir volume.

Figures 8 and 9 present the schematic diagram of the final 3D morphology of hydrofracturing crack networks of multistage horizontal well fracturing. In the multifracturing stage, in stage1, there is no spatial deflection in each case as no interference from adjacent hydrofracturing cracks; in stage 2, gradual deflection to the right occurs due to the accumulation defect of the first hydrofracturing crack; in stage 3, compression deformation phenomena are observed, resulting in more significant spatial

https://doi.org/10.1021/acsomega.3c09641
ACS Omega 2024, 9, 10769−10781

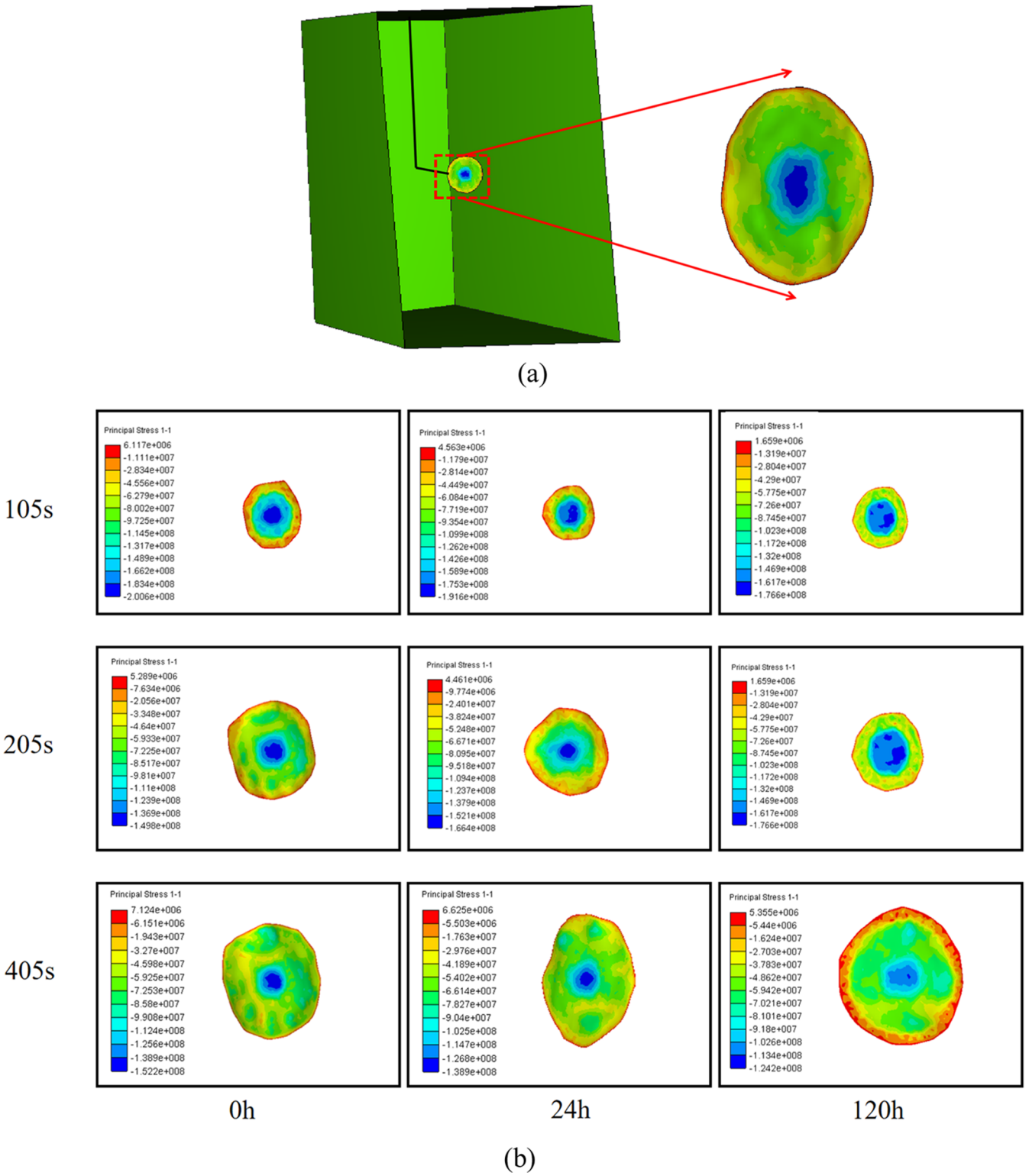

Figure 5. Correlative diagram of single fracturing stage. (a) Schematic diagram of observation angle and (b) morphology of hydrofracturing crack network and σ_1 (Pa) for single fracturing stage.

deflection. At the end of the crack propagation, hydrofracturing crack propagation at 120 h is significantly better than 0 h and 24 h. This is attributed to the reduction of tensile strength σ of the shale reservoir after CO_2 soaking, which decreases the initial hydrofracturing crack pressure, similar to single-stage horizontal well fracturing. Figure 8b demonstrates significant spatial deflection during crack propagation, indicating a strong stress shadow effect. With an increase in cluster spacing, the cracks propagate almost along their initial perforations, resulting in an almost planar final 3D morphology. However, as the soaking time increases, the cracks in the middle positions of the perforation clusters propagate almost entirely along the plane, while deflections of hydrofracturing cracks occur on the symmetric external positions of the perforation clusters. This

https://doi.org/10.1021/acsomega.3c09641
ACS Omega 2024, 9, 10769−10781

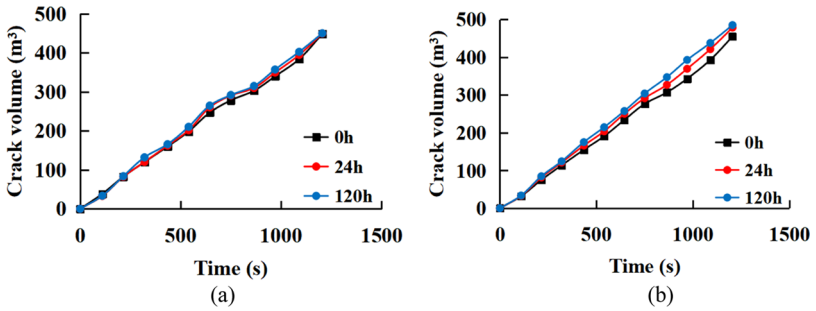

Figure 6. Evolution of hydrofracturing crack volume: (a) cluster space of 25 m and (b) cluster space of 50 m.

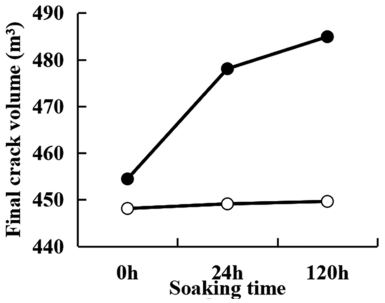

Figure 7. Final hydrofracturing crack volume.

indicates that CO_2 soaking affects the reservoir's permeability and enhances the stress shadow effect, resulting in moderate deflection of hydrofracturing cracks.

The superposition of stress fields between hydrofracturing cracks causes mutual interaction of hydrofracturing cracks during propagation, especially the interaction between shear stress fields.[46] To comprehend the underlying mechanisms governing the development of three-dimensional networks of hydraulic cracks, the evolution of the shear stress field was used to reflect the stress superposition and stress reduction between the hydrofracturing cracks and detect the stress shadow effects. Due to the difference between positive and negative shear stresses on both sides of the hydrofracturing crack, the superposition of different hydrofracturing cracks is easily weakened.[47,48]When the clustering space is 25 m, significant deflection occurs of cracks in all fracturing scenarios due to the interaction of stress fields caused by the narrow cluster spacing. The evolution of shear stress σyz is depicted in Figure 10. In the first stage of fracturing (Figure 10a), the left side of the upper hydrofracturing crack tip exhibits normal shear stress, while the right side shows positive shear stress. Conversely, the left side of the lower hydrofracturing crack tip displays positive shear stress, while the right side exhibits normal values. These stress distributions represent typical patterns observed in the shear stress field surrounding hydrofracturing cracks and are demonstrated nearly symmetric. Consequently, the hydrofracturing cracks propagate in a planar direction without experiencing deflection. Moving on to the stress results of the second stage of fracturing (Figure 10b), the areas of shear stress field variations induced by the propagation of stage 1 notably overlap with those induced by stage 2. As a result, the shear stress field resulting from these first two hydrofracturing cracks undergoes superposition and reduction, weakening the shear stress field on the right side of stage 2. Consequently, stage 2 initiates propagation and deflection toward the left side within the larger stress areas. Based on the same analysis and reasoning, the distribution of the shear stress field for the propagation of stage 3 is shown in Figure 10c,

The shear stress areas of each hydrofracturing crack undergo similar superposition and reduction, causing the cracks to propagate toward the left side within the larger stress areas. This leads to significant defection, as the hydrofracturing crack in the later fracturing sequence more easily encounters larger stress accumulations and experiences more pronounced defection. Furthermore, with an increase in soaking time, the maximum value of the shear stress field in the final crack propagation stage gradually decreases, due to the weakened mechanical properties caused by CO_2 soaking. Consequently, the range of the shear stress field expanded significantly, enhancing the stress shadow effect. At 120 h of soaking, the influence range of the crack's shear stress field expands significantly, which is particularly noticeable. The range of the shear stress field during stages 2 and 3 is significantly larger than in the original state and after 24 h of soaking. Hence, owing to the influence of the stress shadow effect, there is no significant disparity in the volume of crack expansion before and after the soaking process. When the clustering apace is 50 m, the evolution of shear stress σyz is depicted in Figure 11. In the stress results of the first stage of fracturing, as shown in Figure 11a, the left side of the upper hydrofracturing crack tip exhibits normal shear stress, while the right side displays positive values. Conversely, the left side of the lower hydrofracturing crack tip demonstrates positive shear stress, while the right side exhibits normal values. These stress distributions are similar to the case where the cluster spacing is set to 25 m. In the nonsoaking stage, the shear stress field induced by stage 1 did not overlap with the shear stress field induced by stage 2. Consequently, the shear stress fields generated by the first two stages do not superpose, resulting in insignificant deflection of the cracks. However, with the effect of CO_2 soaking, the upper shear stress field region generated by stage 2 affects stage 3. As observed in Figure 11c, the upper portion of stage 3 experiences deflection due to the superposition of shear stress fields. Similar to case 2, an increase in the cluster spacing leads to a gradual decrease in the maximum value of the shear stress field during the final stage of crack expansion. Moreover, the range of the shear stress field contracts significantly, resulting in a weakened stress shadow effect. Consequently, during the later phase of hydraulic fracturing, the presence of CO_2 soaking significantly accelerates the hydrofracturing crack propagation rate, leading to a substantial increase in the final crack volume.

3.3. Discussion. It is evident that CO_2 soaking changes the mechanical properties and permeability of shale oil reservoirs, thereby affecting the practical stimulated reservoir volume. Accurately quantifying these characteristics is crucial for optimizing the design of fracturing stimulation. In order to

https://doi.org/10.1021/acsomega.3c09641
ACS Omega 2024, 9, 10769−10781

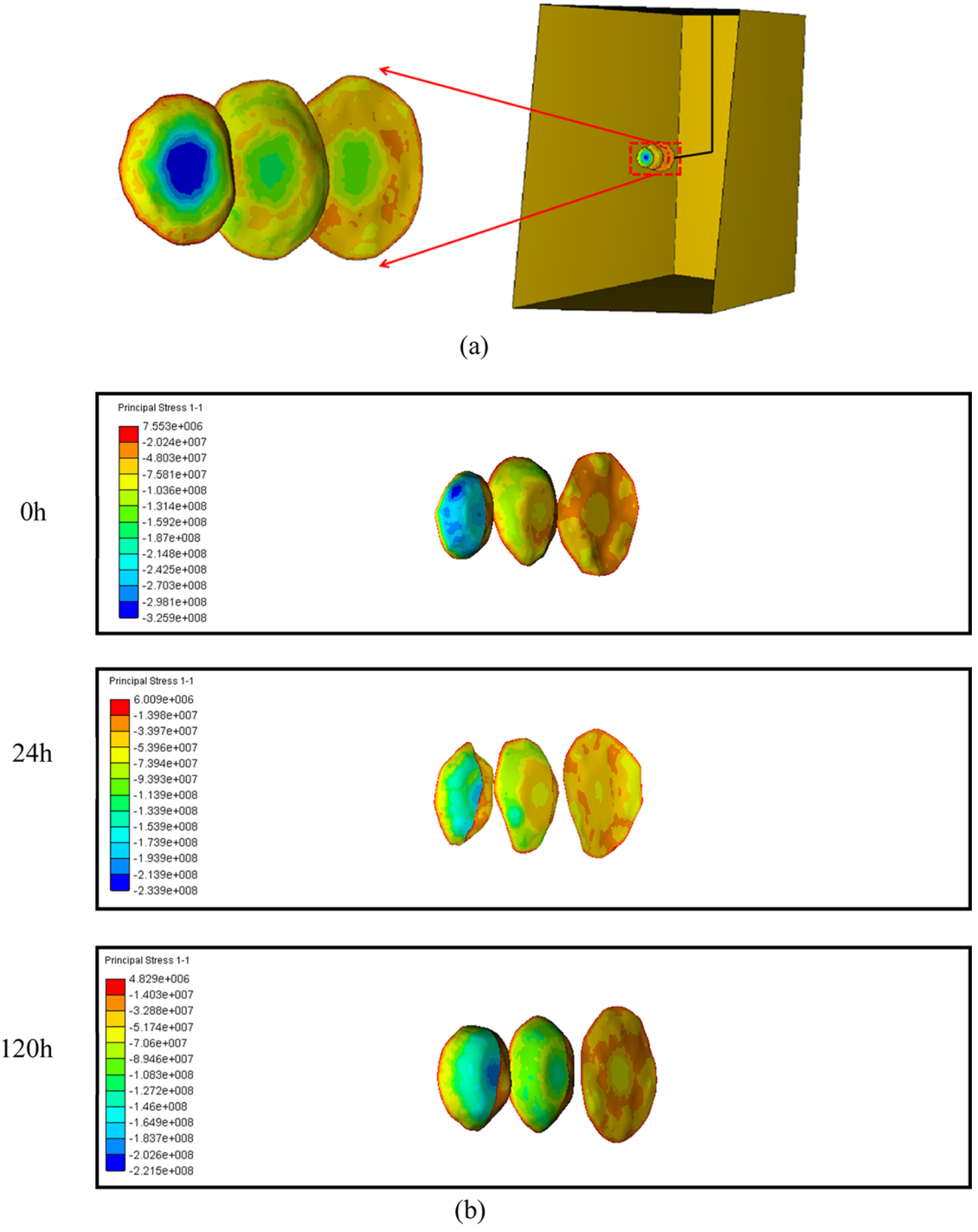

Figure 8. Correlative diagram of multistage fracturing stage:(a) schematic diagram of observation angle and (b) morphology of hydrofracturing crack network and σ_1 (Pa) for 25 m cluster spaces.

better understand the influence of CO_2 soaking on fracturing, a comprehensive evaluation model was developed by introducing a brittleness index (BI). Traditionally, BI has been quantified based on a few mechanical parameters, which limits the accuracy in evaluating reservoir ductility. To address this, the entropy weight method (EWM) was employed in this study to establish a more comprehensive evaluation model for quantitatively determining reservoir brittleness after CO_2 soaking. This method selects the objective relationship between five influencing factors and rock brittleness (Figure 12), and the corresponding weights are chosen. Based on this, an evaluation model as shown in eq 10 is constructed. For more details, we can refer to our previous study.[49]

$$BI = 0.2E^* + 0.32\mu^* + 0.15c^* + 0.15\varphi^* + 0.18\sigma_t^* \quad (10)$$

By utilizing the established comprehensive evaluation model for shale brittleness and selecting relevant experimental data from references (Table 1), we conducted quantitative analysis as depicted in Figure 13. It is observed that the brittleness index of shale oil reservoirs increases with the duration of CO_2 soaking. Based on the analysis of case 1 mentioned earlier, the brittleness and conductivity properties of shale are significantly improved

https://doi.org/10.1021/acsomega.3c09641
ACS Omega 2024, 9, 10769−10781

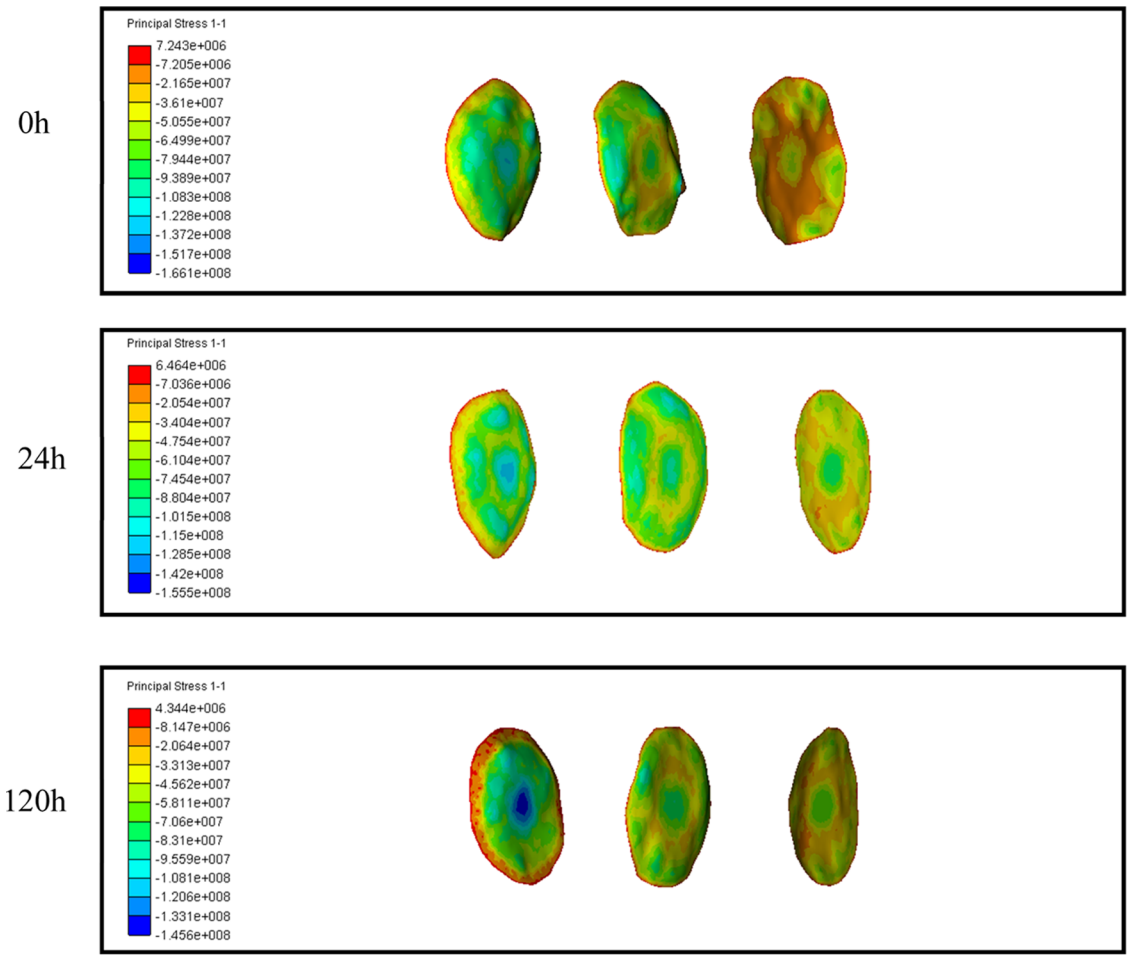

Figure 9. Morphology of hydrofracturing crack network and σ_1 (Pa) for 50 m cluster spaces.

by CO_2 soaking, without considering the stress shadow effect. Consequently, the growth of fractures enters an unstable expansion phase, leading to an increase in the stimulated reservoir volume (SRV), as shown in Figures 4 and 5. At the same time, due to the increased brittleness of the reservoir caused by CO_2 soaking, simultaneously, the increased brittleness of the reservoir resulting from CO_2 soaking makes it easier for hydrofracturing cracks to initiate and propagate within the brittle reservoir and lowers the required pressure for fracturing initiation.

The propagation behavior of hydrofracturing cracks and the impact of stress shadow effects vary due to the cluster spacing set in the initial 3D multistage hydrofracturing model. When the cluster spaces between propagating hydrofracturing cracks are smaller, the stress shadow effects and interaction behaviors between the cracks become more pronounced, leading to a more complex hydrofracturing crack network. This network restrains the development of hydraulic hydrofracturing cracks after the fracturing treatment, thereby negatively affecting the increase in stimulated reservoir volume (SRV). In case 2, where the spaces between propagating hydrofracturing cracks are set to 25 m, significant crack deflection is observed in all fracturing scenarios due to the interaction of stress fields caused by the narrow cluster spacing. Under the combined influence of the stress shadow effect and CO_2 soaking, the volume of hydrofracturing cracks tends to increase with the soaking time but remains lower compared to case 3. Although the increase in reservoir brittleness caused by pre-injection of CO_2 can enhance the SRV, its impact is not significant under the dominant stress shadow effect when the cluster space is too narrow. In case 3, the stress shadow effect becomes noticeably weaker compared to case 2 with an increase in cluster spacing. As a result, the expansion volume of hydrofracturing cracks significantly increases. After CO_2 injection, the shear stress field becomes complicated due to the CO_2 soaking. The enhanced stress shadow effect leads to moderate crack deflection. However, CO_2 soaking has a more obvious effect on rock brittleness and electrical conductivity, resulting in a continuous increase in SRV.

4. CONCLUSIONS

This article reviews the current laboratory experiment research on the effect of CO_2 soaking on shale permeability and mechanical properties. Considering that CO_2 soaking changes the mechanical and permeability properties of shale reservoirs, we based on the adaptive finite element−discrete element method, considering factors such as fluidic-mechanical-crack coupling mechanisms and leakage effects, the hydraulic fracturing simulation of shale oil reservoir under different CO_2 soaking time is carried out. The results revealed the spatial distribution characteristics of a three-dimensional hydraulic crack network in shale oil reservoirs with other CO_2 soaking times. Finally, we introduce the comprehensive evaluation model of the elastic-plastic reservoir created by our research group. The influence of CO_2 soaking time on the brittleness characteristics of shale reservoir was quantitatively analyzed to

https://doi.org/10.1021/acsomega.3c09641
ACS Omega 2024, 9, 10769−10781

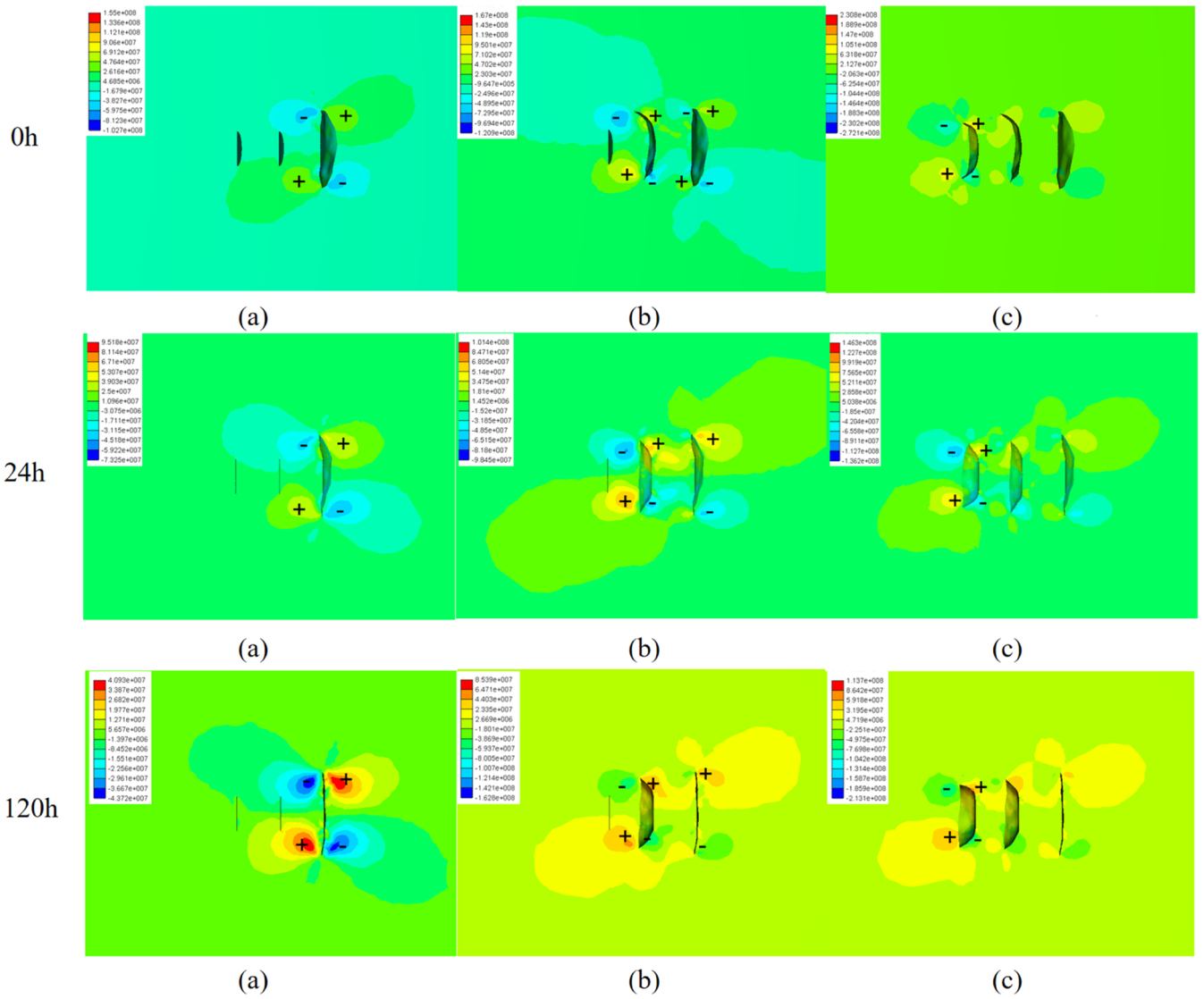

Figure 10. Evolution of shear stress σ_{yz} (Pa) for cluster space of 25 m (note: "+" represents positive shear stress and "−" represents negative shear stress): (a) 1st-stage fracturing, (b) 2nd-stage fracturing, (c) 3rd-stage fracturing.

make a comprehensive evaluation of hydraulic fracturing. The main conclusions are as follows:

1. Considering that CO_2 soaking changes the permeability and conductivity properties of shale reservoirs, which leads to the fluid−solid coupling effect, we adopt an adaptive finite element−discrete element method that incorporates mechanical-crack coupling mechanism and leakage effects to simulate 3D hydraulic fracturing of shale oil reservoirs after different CO_2 soaking time. We conducted three groups of horizontal well fracturing cases with varying spacing of clusters to study the effect of preinjected CO_2 on the hydraulic fracturing behavior of shale oil reservoirs.
2. The comprehensive evaluation model of the elastic-plastic reservoir created by our research group has been used to determine the brittleness of reservoirs after CO_2 soaking quantitatively. We considered elastic modulus, Poisson's ratio, cohesion, internal friction angle, and tensile strength as five mechanical parameters. At the same time, the porosity and permeability of SC−CO_2 soaking matrix shale were quantified according to the biot coefficient (α) by the empirical formula. We found that with the increase of CO_2 soaking time, the brittleness index and the biot coefficient of shale oil reservoirs increase, which means both the brittleness and conductivity properties of shale rock are dramatically improved as the increment of soaking time of CO_2.
3. The results indicate that both the brittleness and conductivity properties of shale rock are dramatically improved as the increment of soaking time of CO_2 that the effect of stress shadow is not considered. Thus, improving the brittleness index is beneficial to improve the SRV and the initiation pressure is reduced with the increment of soaking time of CO_2. After CO_2 soaking for a long time, the increase of conductivity affects the shear stress field of crack growth, enhances the stress shadow effect of crack, and reduces the crack growth volume. Thus, as the stress shadow effect is involved in the horizontal well fracturing, the complexity of the hydro-fracturing crack is significantly enhanced to restrain the development of hydrofracturing crack after hydraulic fracturing treatment, especially when the cluster spacing is

https://doi.org/10.1021/acsomega.3c09641
ACS Omega 2024, 9, 10769−10781

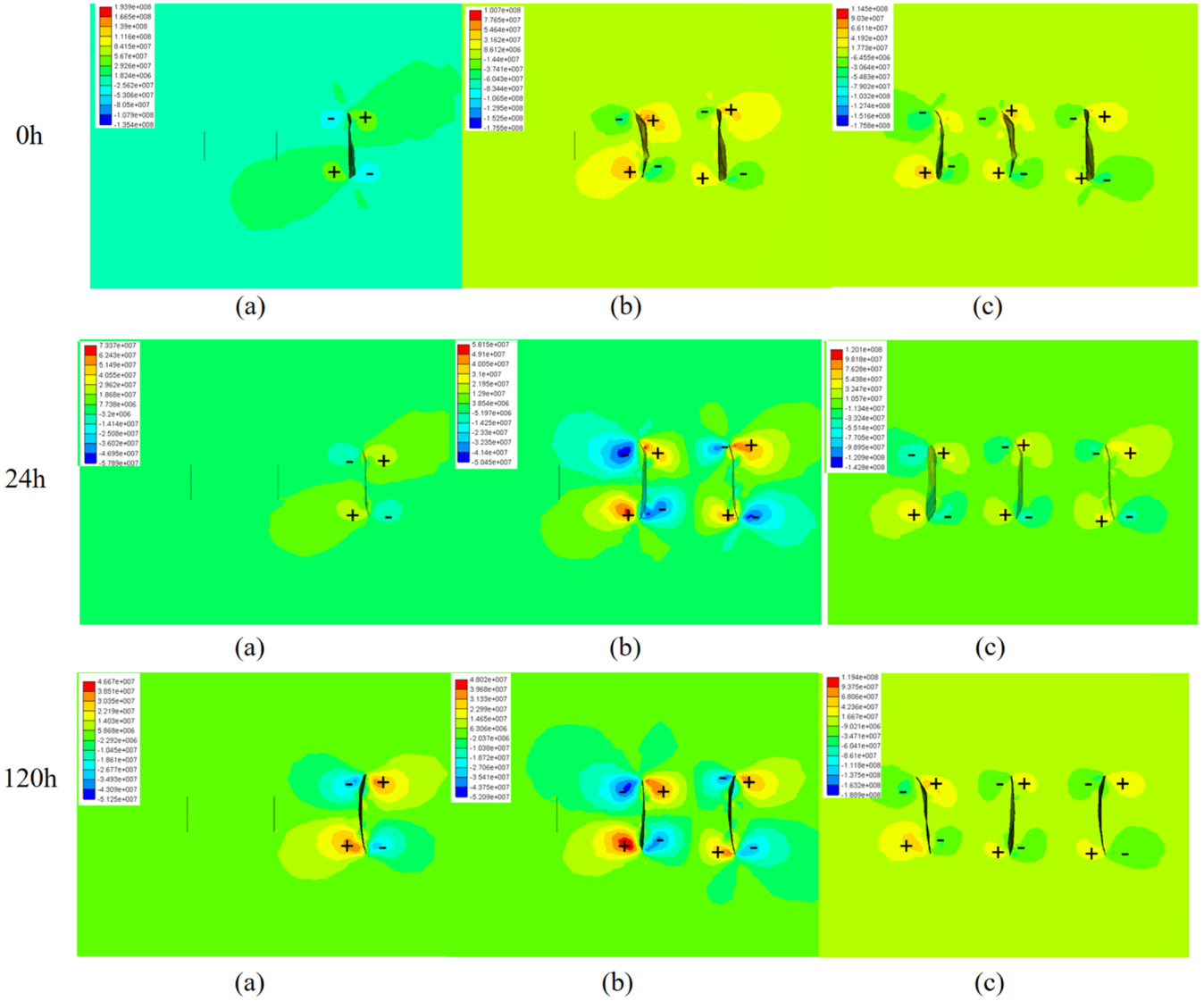

Figure 11. Evolution of shear stress σ_{yz} (Pa) for cluster space of 50 m (note: "+" represents positive shear stress and "−" represents negative shear stress). (a) 1st-stage fracturing, (b) 2nd-stage fracturing, (c) 3rd-stage fracturing.

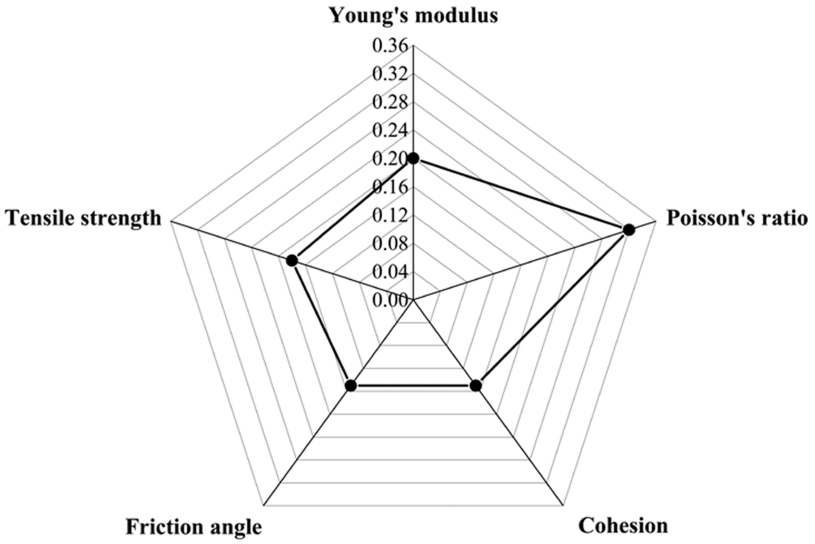

Figure 12. Weight of the influence of various factors on shale oil reservoirs.

https://doi.org/10.1021/acsomega.3c09641
ACS Omega 2024, 9, 10769−10781

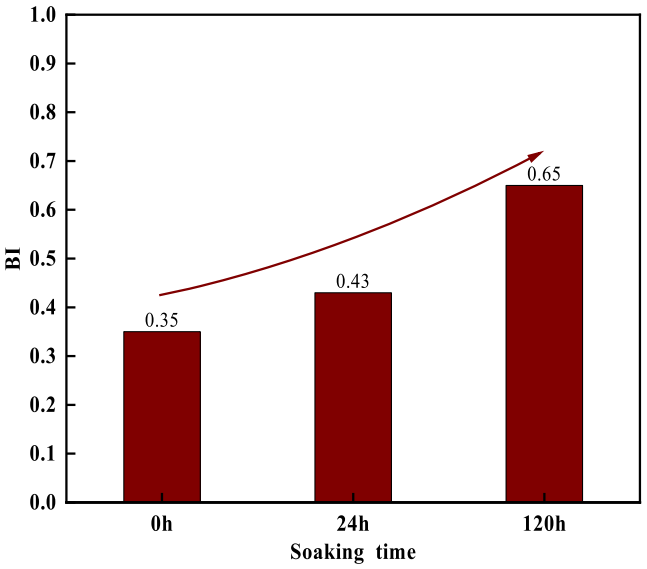

Figure 13. Evaluation of brittleness index under different CO_2 soaking times.

narrow. When the cluster spacing is larger, the stress shadow effect is weakened, and the weakening effect of CO_2 soaking on rock reservoir is more obvious. After CO_2 prefracturing, the reservoir SRV is greatly increased.

AUTHOR INFORMATION

Corresponding Author

Yi Ding − *University of Newcastle, Newcastle 2308, Australia; School of Mechanics and Civil Engineering, China University of Mining and Technology, Beijing 100083, China;* orcid.org/0000-0001-7830-9516; Email: yd195@newcastle.edu.au

Authors

Hang Yu − *School of Energy and Mining, China University of Mining and Technology, Beijing 100083, China*

Yuyang Wang − *School of Energy and Mining, China University of Mining and Technology, Beijing 100083, China*

Wenlong Zhou − *School of Energy and Mining, China University of Mining and Technology, Beijing 100083, China;* orcid.org/0009-0001-7972-4460

Complete contact information is available at: https://pubs.acs.org/10.1021/acsomega.3c09641

Notes

The authors declare no competing financial interest.

ACKNOWLEDGMENTS

The authors thank the China Scholarship Council (grant number 845629), which supports this work, and are grateful to the two anonymous reviewers for their valuable comments and suggestions.

REFERENCES

(1) Melikoglu, M. Shale gas: Analysis of its role in the global energy market. *Renewable Sustainable Energy Rev.* **2014**, *37*, 460−468.

(2) Zou, C.; Zhao, Q.; Zhang, G.; Xiong, B. Energy revolution: From a fossil energy era to a new energy era. *Nat. Gas Ind. B* **2016**, *3* (1), 1−11.

(3) Mansoor, R.; Tahir, M. Recent developments in natural gas flaring reduction and reformation to energy-efficient fuels: a review. *Energy Fuels* **2021**, *35* (5), 3675−3714.

(4) Lau, H. C.; Li, H.; Huang, S. Challenges and opportunities of coalbed methane development in China. *Energy Fuels* **2017**, *31* (5), 4588−4602.

(5) Zhang, H.; Sheng, J. Optimization of horizontal well fracturing in shale gas reservoir based on stimulated reservoir volume. *J. Pet. Sci. Eng.* **2020**, *190*, No. 107059.

(6) Zhang, R.-h.; Zhang, L.-h.; Tang, H.-y.; Chen, S.-n.; Zhao, Y.-l.; Wu, J.-f.; Wang, K.-r. A simulator for production prediction of multistage fractured horizontal well in shale gas reservoir considering complex fracture geometry. *J. Nat. Gas Sci. Eng.* **2019**, *67*, 14−29.

(7) Hou, B.; Chen, M.; Li, Z.; Wang, Y.; Diao, C. Propagation area evaluation of hydraulic fracture networks in shale gas reservoirs. *Pet. Explor. Dev.* **2014**, *41* (6), 833−838.

(8) Ju, X.; Liu, F.; Fu, P.; White, M. D.; Settgast, R. R.; Morris, J. P. Gas production from hot water circulation through hydraulic fractures in methane hydrate-bearing sediments: THC-coupled simulation of production mechanisms. *Energy Fuels* **2020**, *34* (4), 4448−4465.

(9) Ribeiro, L. H.; Li, H.; Bryant, J. E. Use of a CO2-Hybrid Fracturing Design To Enhance Production From Unpropped-Fracture Networks. *SPE Prod. Oper.* **2017**, *32* (1), 28−40.

(10) Song, C.; Yang, D. Experimental and numerical evaluation of CO2 huff-n-puff processes in Bakken formation. *Fuel* **2017**, *190*, 145−162.

(11) Li, B.; Mou, J.; Zhang, S.; Ma, X.; Zou, Y.; Wang, F. Experimental Study on the Interaction Between CO2 and Rock During CO2 Pre-pad Energized Fracturing Operation in Thin Interbedded Shale. *Front. Energy Res.* **2022**, *10*, No. 825464, DOI: 10.3389/fenrg.2022.825464.

(12) Huang, L.; Zhou, W.; Xu, H.; Wang, L.; Zou, J.; Zhou, Q. Dynamic fluid states in organic-inorganic nanocomposite: Implications for shale gas recovery and CO2 sequestration. *Chem. Eng. J.* **2021**, *411*, No. 128423.

(13) Guo, T.; Gong, F.; Wang, X.; Lin, Q.; Qu, Z.; Zhang, W. Performance of enhanced geothermal system (EGS) in fractured geothermal reservoirs with CO2 as working fluid. *Appl. Therm. Eng.* **2019**, *152*, 215−230.

(14) Lin, R.; Yu, Z.; Zhao, J.; Dai, C.; Sun, Y.; Ren, L.; Xie, M. Experimental evaluation of tight sandstones reservoir flow characteristics under CO2−Brine−Rock multiphase interactions: A case study in the Chang 6 layer, Ordos Basin, China. *Fuel* **2022**, *309*, No. 122167.

(15) Lu, Y.; Zhou, J.; Li, H.; Tang, J.; Zhou, L.; Ao, X. Gas flow characteristics in shale fractures after supercritical CO2 soaking. *J. Nat. Gas Sci. Eng.* **2021**, *88*, No. 103826, DOI: 10.1016/j.jngse.2021.103826.

(16) Ishida, T.; Aoyagi, K.; Niwa, T.; Chen, Y.; Murata, S.; Chen, Q.; Nakayama, Y. Acoustic emission monitoring of hydraulic fracturing laboratory experiment with supercritical and liquid CO2 *Geophys. Res. Lett.* 2012, *39*, 16.

(17) Li, S.; Zhang, S.; Zou, Y.; Zhang, X.; Ma, X.; Wu, S.; Zhang, Z.; Sun, Z.; Liu, C. Experimental study on the feasibility of supercritical CO2-gel fracturing for stimulating shale oil reservoirs. *Eng. Fract. Mech.* **2020**, *238*, No. 107276, DOI: 10.1016/j.engfracmech.2020.107276.

(18) Zhang, X.; Wei, B.; Shang, J.; Gao, K.; Pu, W.; Xu, X.; Wood, C.; Sun, L. Alterations of geochemical properties of a tight sandstone reservoir caused by supercritical CO2-brine-rock interactions in CO2-EOR and geosequestration. *J. CO2 Util.* **2018**, *28*, 408−418.

(19) Qin, C.; Jiang, Y.; Zhou, J.; Zuo, S.; Chen, S.; Liu, Z.; Yin, H.; Li, Y. Influence of supercritical CO2 exposure on water wettability of shale: Implications for CO2 sequestration and shale gas recovery. *Energy* **2022**, *242*, No. 122551, DOI: 10.1016/j.energy.2021.122551.

(20) Ding, M.; Wang, Y.; Han, Y.; Gao, M.; Wang, R. Interactions in bypassed oil-CO2 systems and their utilization in enhancing the recovery of bypassed oil. *Fuel* **2019**, *237*, 1068−1078.

(21) Abedini, A.; Torabi, F. On the CO2 storage potential of cyclic CO2 injection process for enhanced oil recovery. *Fuel* **2014**, *124*, 14−27.

(22) Nobakht, M.; Moghadam, S.; Gu, Y. Mutual interactions between crude oil and CO2 under different pressures. *Fluid Phase Equilib.* **2008**, *265* (1−2), 94−103.

(23) Lei, X.; et al. Role of drainage conditions in deformation and fracture of porous rocks under triaxial compression in the laboratory. *Geophys. Res. Lett.* **2011**, *38*, No. L24310.
(24) Pan, Y.; Hui, D.; Luo, P.; Zhang, Y.; Sun, L.; Wang, K. Experimental Investigation of the Geochemical Interactions between Supercritical CO2 and Shale: Implications for CO2 Storage in Gas-Bearing Shale Formations. *Energy Fuels* **2018**, *32* (2), 1963−1978.
(25) Pan, Y.; Hui, D.; Luo, P.; Zhang, Y.; Zhang, L.; Sun, L. Influences of subcritical and supercritical CO2 treatment on the pore structure characteristics of marine and terrestrial shales. *J. CO2 Util.* **2018**, *28*, 152−167.
(26) Jiang, Z.; Wang, W.; Zhu, H.; Yin, Y.; Qu, Z. Review of Shale Gas Transport Prediction: Basic Theory, Numerical Simulation, Application of AI Methods, and Perspectives. *Energy Fuels* **2023**, *37* (4), 2520−2538.
(27) Balsamo, S.; Di Marco, A.; Inverardi, P.; Simeoni, M. Model-based performance prediction in software development: A survey. *IEEE Trans. Soft. Eng.* **2004**, *30* (5), 295−310.
(28) Jeruchim, M. C.; Balaban, P.; Shanmugan, K. S. *Simulation of Communication Systems: Modeling, Methodology and Techniques*; Springer Science & Business Media, 2006.
(29) Li, L.; Li, J.; Li, G.; Tan, Y.; Chen, X.; Ren, F.; Guo, H.; Wang, H. A tetraploid minimally differentiated acute myeloblastic leukemia with extensive erythrophagocytosis: a case report and literature review. *Int. J. Hematol.* **2012**, *96*, 801−805.
(30) Abdelaziz, A.; Ha, J.; Li, M.; Magsipoc, E.; Sun, L.; Grasselli, G. Understanding hydraulic fracture mechanisms: From the laboratory to numerical modelling. *Adv. Geo-Energy Res.* **2023**, *7* (1), 66−68.
(31) Kim, J.; Lee, J. Y.; Ahn, T. W.; Yoon, H. C.; Lee, J.; Yoon, S.; Moridis, G. J. Validation of strongly coupled geomechanics and gas hydrate reservoir simulation with multiscale laboratory tests. *Int. J. Rock Mech. Min. Sci.* **2022**, *149*, No. 104958.
(32) Guo, X.; Jin, Y.; Zi, J.; Lin, J.; Zhu, B. A 3D modeling study of effects of heterogeneity on system responses in methane hydrate reservoirs with horizontal well depressurization. *Gas Sci. Eng.* **2023**, *115*, No. 205001.
(33) Wang, Y.; Ju, Y.; Chen, J.; Song, J. Adaptive finite element−discrete element analysis for the multistage supercritical CO2 fracturing and microseismic modelling of horizontal wells in tight reservoirs considering pre-existing fractures and thermal-hydro-mechanical coupling. *J. Nat. Gas Sci. Eng.* **2019**, *61*, 251−269.
(34) Wang, Y.; Ju, Y.; Zhang, H.; Gong, S.; Song, J.; Li, Y.; Chen, J. Adaptive Finite Element−Discrete Element Analysis for the Stress Shadow Effects and Fracture Interaction Behaviours in Three-Dimensional Multistage Hydrofracturing Considering Varying Perforation Cluster Spaces and Fracturing Scenarios of Horizontal Wells. *Rock Mech. Rock Eng.* **2021**, *54* (4), 1815−1839.
(35) Wang, Y.; Liu, N.; Zhang, X.; Liu, X.; Wang, J. Influences on unstable hydraulic fractures: propagation of adjacent multiple perforations and bedded interfaces in multilayered reservoir via FE-DE model. *Eng. Comput.* **2022**, *39* (4), 1407−1431.
(36) Ju, Y.; Wang, Y.; Chen, J.; Gao, F.; Wang, J. Adaptive finite element-discrete element method for numerical analysis of the multistage hydrofracturing of horizontal wells in tight reservoirs considering pre-existing fractures, hydromechanical coupling, and leak-off effects. *J. Nat. Gas Sci. Eng.* **2018**, *54*, 266−282.
(37) Ju, Y.; Li, Y.; Wang, Y.; Yang, Y. Stress shadow effects and microseismic events during hydrofracturing of multiple vertical wells in tight reservoirs: A three-dimensional numerical model. *J. Nat. Gas Sci. Eng.* **2020**, *84*, No. 103684, DOI: 10.1016/j.jngse.2020.103684.
(38) Profit, M.; Dutko, M.; Yu, J.; Cole, S.; Angus, D.; Baird, A. Complementary hydro-mechanical coupled finite/discrete element and microseismic modelling to predict hydraulic fracture propagation in tight shale reservoirs. *Comput. Part. Mech.* **2016**, *3* (2), 229−248.
(39) Lobao; Centeno, M. *Finite Element Modelling of Hydraulic Fracture Flow in Porous Media*; Swansea University, 2007.
(40) Williams, B. B. Fluid Loss from Hydraulically Induced Fractures. *J. Pet. Technol.* **1970**, *22* (07), 882.
(41) Howard, G.; Fast, C. R. Optimum Fluid Characteristics for Fracture Extension. In *Drilling & Production Practice*; OnePetro, 1957.
(42) Ao, X.; Lu, Y.; Tang, J.; Chen, Y.; Li, H. Investigation on the physics structure and chemical properties of the shale treated by supercritical CO 2. *J. CO2 Util.* **2017**, *20*, 274−281.
(43) Lyu, Q.; Wang, K.; Wanniarachchi, W. A. M.; Hu, C.; Shi, J. Hydro-Mechanical Properties of a Low-Clay Shale with Supercritical CO2 Imbibition. In *Geomechanics and Geophysics for Geo-Energy and Geo-Resources*; Springer, 2020; Vol. *6*.
(44) Haitao, W.; Luo, Z.; Yintong, G. Effect of carbon dioxide on the degradation of shale mechanical properties. *Sci. Technol. Eng.* **2021**, *21* (29), 12536−12542.
(45) Li, Q.; Aguilera, R.; Cinco-Ley, H. A Correlation for Estimating the Biot Coefficient. *SPE Drill. Completion* **2020**, *35* (02), 151−163.
(46) He, Q.; Suorineni, F. T.; Ma, T.; Oh, J. Effect of discontinuity stress shadows on hydraulic fracture re-orientation. *Int. J. Rock Mech. Min. Sci.* **2017**, *91*, 179−194.
(47) Yoon, J. S.; Zimmermann, G.; Zang, A. Numerical Investigation on Stress Shadowing in Fluid Injection-Induced Fracture Propagation in Naturally Fractured Geothermal Reservoirs. *Rock Mech. Rock Eng.* **2015**, *48* (4), 1439−1454.
(48) Taghichian, A.; Zaman, M.; Devegowda, D. Stress shadow size and aperture of hydraulic fractures in unconventional shales. *J. Pet. Sci. Eng.* **2014**, *124*, 209−221.
(49) Ju, Y.; Wu, G.; Wang, Y.; Liu, P.; Yang, Y. 3D Numerical Model for Hydraulic Fracture Propagation in Tight Ductile Reservoirs, Considering Multiple Influencing Factors via the Entropy Weight Method. *SPE J.* **2021**, *26*, 2685−2702.

https://doi.org/10.1021/acsomega.3c09641
ACS Omega 2024, 9, 10769−10781